CJC Chinese Journal of Chemistry 中国化学 - An International Journal

For submission: https://wiley.atyponrex.com/journal/CJOC
For published articles: https://onlinelibrary.wiley.com/journal/16147065

Concise Report

Cite this paper: *Chin. J. Chem.* **2025**, *43*, 791—797. **DOI: 10.1002/cjoc.202400905**

Efficient Photothermal CO Hydrogenation into C_{2+} Hydrocarbons on *in situ* Generated Fe^0 in Fe_5C_2 Active Sites via Cu-Promoted Hydrogen Dissociation and Spillover†

Renjie Zhou, Haoyang Jiang, Yongcheng Xiao, Yueren Liu, and Miao Zhong*

College of Engineering and Applied Sciences, Collaborative Innovation Center of Advanced Microstructure, National Laboratory of Solid State Microstructures, the Frontiers Science Center for Critical Earth Material Cyclings, Nanjing University, Nanjing, Jiangsu 210023, China

Keywords

Photothermal catalysis | Fischer–Tropsch synthesis | Hydrogen spillover | Fe_5C_2 | Product distribution | Hydrocarbons | Catalytic activity | Supported catalysts

Comprehensive Summary

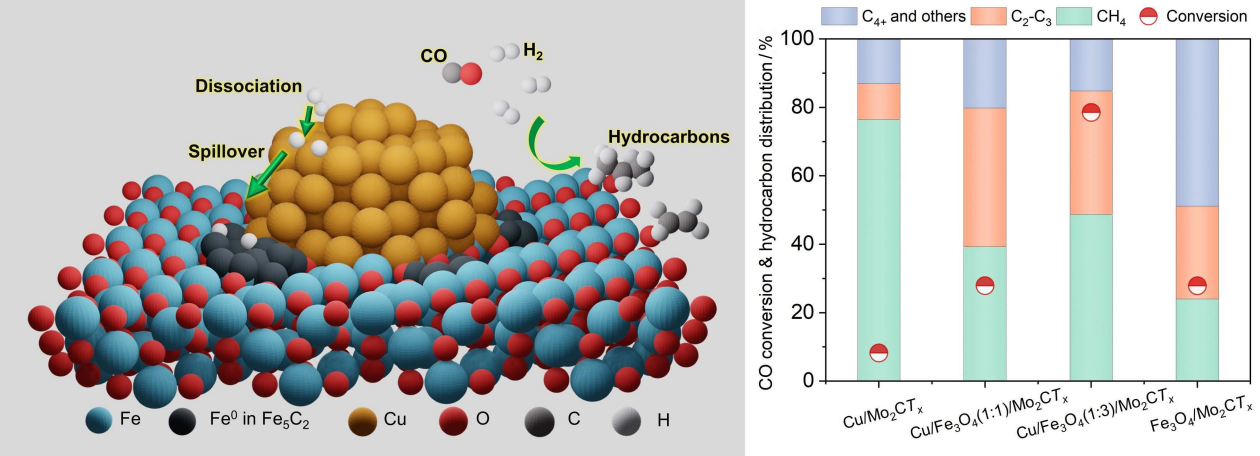

Photothermal hydrogenation of carbon monoxide (CO) holds the potential to generate valuable C_{2+} chemicals using renewable solar energy. However, its activity and selectivity towards C_2—C_3 alkanes are limited compared to conventional thermal catalysis. In this study, we developed a robust catalyst consisting of Cu/Fe_3O_4 nanoparticles on Mo_2CT_x MXene, showing enhanced photothermal C_2—C_3 production. The Cu component plays a crucial role in H_2 dissociation and subsequent H spillover, facilitating the *in situ* generation of Fe^0 in Fe_5C_2 active sites and thus efficiently promoting photothermal CO hydrogenation. As a result, we achieved a 51.3% C_{2+} selectivity and 78.5% CO conversion at a high gas hourly space velocity (GHSV) of 12000 $mL \cdot g_{cat}^{-1} \cdot h^{-1}$ and 2.5 MPa in a flow reactor at 320 °C. The overall C_2—C_3 yield reached 23.6% with $Cu/Fe_3O_4/Mo_2CT_x$ catalysts, marking a 2.8-fold increase compared to the performance of the bare Fe_3O_4/Mo_2CT_x catalyst.

*E-mail: miaozhong@nju.edu.cn
† Dedicated to the Special Issue of Emerging Investigators in 2024.

Background and Originality Content

Fischer-Tropsch synthesis (FTS), a process that converts syngas (CO and H_2) into valuable C_{2+} hydrocarbon fuels and chemicals, has been extensively studied.[1] However, conventional FTS operations require high temperatures above 350 °C, resulting in substantial consumption of fossil fuels and significant CO_2 emissions. An alternative approach is to utilize solar energy as the driving force for the FTS reaction.[2] Industrial FTS catalysts, typically iron or cobalt-based materials, exhibit a dark color, enabling absorption across a broad spectrum of solar light.[3-5] Under concentrated solar light irradiation, these catalysts can reach temperatures of several hundred degrees Celsius, which is sufficient for the FTS reaction.[3,6]

Recently, Ma and colleagues[7] developed an Iron (Fe)-based catalyst, showing a high selectivity of 55.5% for C_2—C_4 olefins with ~49% CO conversion in a 30-min photothermal batch reaction. The process exhibited an olefin/paraffin ratio of 10.9 and a low CO_2 selectivity (18.9%). The active phase responsible for CO dissociation and C—C coupling was identified as Fe_5C_2.[8-10] Li *et al.*[11] reported a hydrophobic core-shell Fe-based FTS catalyst, which enhanced CO hydrogenation while suppressing the water-gas shift side reaction, achieving an excellent selectivity of 48.0% for light olefins ($C_{2-4}^{=}$) and a CO conversion of 22.6%. Additionally, researchers designed a cobalt ferrite ($CoFe_2O_4$) spinel catalyst[12] to produce C_2—C_4 hydrocarbons through photothermal CO_2-FTS, demonstrating that the alloy-spinel nanocomposite facilitated the light-assisted transformation of CO_2 to CO and the subsequent hydrogenation of CO. Based on this success, further efforts are expected to enhance productivity while maintaining catalytic stability at operating temperatures, such as 350 °C.[3]

Copper (Cu) has a wide range of applications in various photothermal catalytic reactions.[13-14] Studies have revealed that the mechanism of CO hydrogenation into hydrocarbons over Cu-based composites differs from conventional FTS, and the hydrocarbon products are therefore not limited by the Anderson–Schulz–Flory (ASF) distribution.[15] Additionally, the reported results show that the introduction of Cu improves the stability of Fe-based catalysts by facilitating the regeneration of FTS active sites during the reaction.[16] More importantly, Cu sites are attributed to a high affinity for H_2 activation, hence, increasing the concentration of dissociated hydrogen on the catalyst surface to assist in the reduction of iron oxides.[17-18]

Mo_2CT_x (MXene), with a general formula of $M_{n+1}X_nT_x$ (where n = 1, 2, 3, X represents C and/or N, and T represents surface –O–, –OH and/or –F groups), emerges as an effective catalyst support for photothermal reactions due to its broad-band light absorption and efficient photo-to-thermal conversion heater.[19-20-22] Additionally, Mo_2CT_x is predicted to be effective for CO_2 capture, storage, and activation,[20,23] and has been employed in CO_2 hydrogenation for CO and methanol synthesis.[24]

In this work, we fabricated Cu-loaded Fe_3O_4 (Cu/Fe_3O_4) catalysts on a multilayered Mo_2CT_x support and reported on the photothermal CO hydrogenation into C_{2+} hydrocarbons. The selectivity for C_{2+} hydrocarbons exceeded 51% with a high CO conversion of 78.5% under 300 W Xenon light irradiation (for a surface temperature of 346 °C) and external heating (for a bulk temperature of 320 °C) at 2.5 MPa. Particularly, the photothermal selectivity for C_2H_6 and C_3H_8 (C_2—C_3 alkanes) approached 40% at a high gas hourly space-time velocity (GHSV) of 12000 $mL \cdot g_{cat}^{-1} \cdot h^{-1}$. Our findings indicate that Cu activates H_2 molecules, which subsequently spill over to the Fe^{3+}, facilitating its *in situ* reduction to produce the active Fe^0 in Fe_5C_2 centers and promote C_{2+} generation.

Results and Discussion

Figures 1a and b present the narrow-scan X-ray photoelectron spectroscopy (XPS) of the catalysts before and after the photothermal CO hydrogenation reaction, respectively. The XPS spectra of Fe 2p for Cu/Fe_3O_4(1:1)/Mo_2CT_x, Cu/Fe_3O_4(1 : 3)/Mo_2CT_x and Fe_3O_4/Mo_2CT_x exhibited binding energies of Fe $2p_{3/2}$ and Fe $2p_{1/2}$ at ~710.8 and ~724.0 eV, respectively (Figure 1a). They contained Fe^{3+} and Fe^{2+} species. Notably, the post-reaction $Cu/Fe_3O_4/Mo_2CT_x$ (Cu : Fe = 1 : 1 and 1 : 3, Figure 1b) showed additional peaks which were attributed to the presence of Fe^0 species in the Fe $2p_{3/2}$ and Fe $2p_{1/2}$ spectrum compared to the fresh samples (Figure 1a). This indicated the generation of Fe^0 species on $Cu/Fe_3O_4/Mo_2CT_x$ during the reaction. In contrast, no Fe^0 peak was observed with the post-reaction Fe_3O_4/Mo_2CT_x catalyst. These results suggested that Cu plays an essential role in the reduction of Fe^{3+} to Fe^0 during the reaction.

Figure S1 show the detailed-scan XPS spectra of the Cu/Mo_2CT_x, Cu/Fe_3O_4(1 : 1)/Mo_2CT_x and Cu/Fe_3O_4(1 : 3)/Mo_2CT_x catalysts before and after the reaction. Both Cu and Cu^{2+} were identified. We suggest that during the reaction, Cu^{2+} is first reduced to Cu^0. The generated Cu^0 facilitates H_2 dissociation into H on its surface, and then spills over to Fe species, contributing to the formation of the active Fe^0 species.

The satellite peaks observed at 719.1 eV for Fe $2p_{3/2}$ correspond to Fe_2O_3, rather than Fe_3O_4, which has been confirmed by a previous study comparing the XPS spectra between Fe_2O_3 and Fe_3O_4.[25] The fitted XPS spectra of Cu 2p (Figure S1) show two prominent peaks at 925—936 eV attributed to Cu $2p_{3/2}$, and 946—957 eV attributed to Cu $2p_{1/2}$. The peaks with binding energy lower than 932.5 eV were assigned to Cu^0, while the peaks at 942.5 and 961.5 eV were probably the satellite signals of Cu^{2+}. The characteristic shakeup satellites were attributed to the charge transfer between the 3d orbitals of transition metal and the 2p orbitals of surrounding oxygen ligands.[26]

Figure 1c displays the XRD patterns of Cu/Fe_3O_4(1 : 1)/Mo_2CT_x, Cu/Fe_3O_4(1 : 3)/Mo_2CT_x, Cu/Mo_2CT_x, and Fe_3O_4/Mo_2CT_x. Except for Cu/Mo_2CT_x, the diffraction peaks at 35.5° and 62.6° were observed in all the catalysts, indicating the presence of Fe_3O_4 phases. In the $Cu/Fe_3O_4/Mo_2CT_x$ catalysts, the peaks of metallic Cu at 43.4° and 50.5° were observed, suggesting the formation of phase-separated Cu/Fe_3O_4 composite. In order to clearly observe the phase transformation of Fe-related species without the interference of other diffraction peaks, we loaded Fe_3O_4 and Cu/Fe_3O_4 on SiO_2 using the identical synthesis method. The reaction time was extended to 30 h for the catalysts Fe_3O_4/SiO_2 and $Cu/Fe_3O_4/SiO_2$, under the same reaction conditions as MXene-based catalysts. As depicted in Figure 1d, after a 30-hour reaction, Fe species in Cu/Fe_3O_4 sample completely transformed to Fe_5C_2, while in the Fe_3O_4 sample, it only partially transformed into Fe_5C_2. This observation confirms that the presence of Cu facilitates the *in situ* generation of Fe-based carbide active centers.

The optical properties of the MXene-supported catalysts were examined using ultraviolet-visible–infrared (UV-Vis-NIR) absorption spectroscopy (Figure S2). All the catalysts display a strong absorbance over a wide wavelength range of 350—2350 nm, which implies a high utilization efficiency of solar energy by MXene-supported catalysts. The scanning electron microscopy (SEM) and energy-dispersive X-ray spectroscopy mapping (EDS) images of Mo_2CT_x MXene and the best-performing Cu/Fe_3O_4(1 : 3)/Mo_2CT_x catalyst are shown in Figure 2. Fe and Cu were uniformly distributed on the Mo_2CT_x surface. The transmission electron microscopy (TEM) image with (EDX) (Figure S3) shows that the Cu and Fe_3O_4 particles are highly dispersed throughout Mo_2CT_x, and the High-resolution (HR)-TEM image displays the presence of the Cu/Fe_3O_4 interface.

The phenomenon of hydrogen spillover from Cu to FeO_x was validated using the chromism of WO_3 (Figure 3 and Figure S4). The process is as follows: after uniformly mixing the catalyst sample with WO_3, it is subjected to treatment under heat and a hydrogen atmosphere. If hydrogen dissociation and spillover occur, the

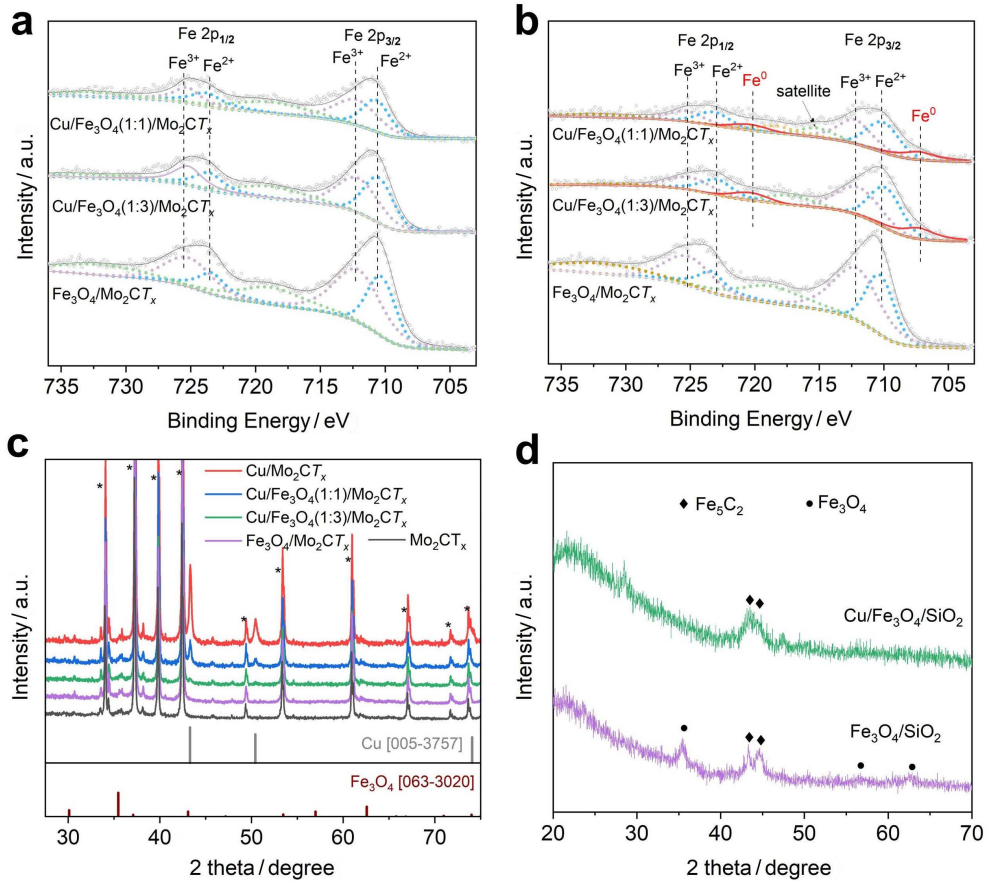

Figure 1 XPS results of Fe 2p from the catalysts before (a) and after a 6-h reaction (b); (c) XRD patterns of the catalysts; (d) XRD patterns of the catalysts supported on SiO_2 after a 30-h reaction.

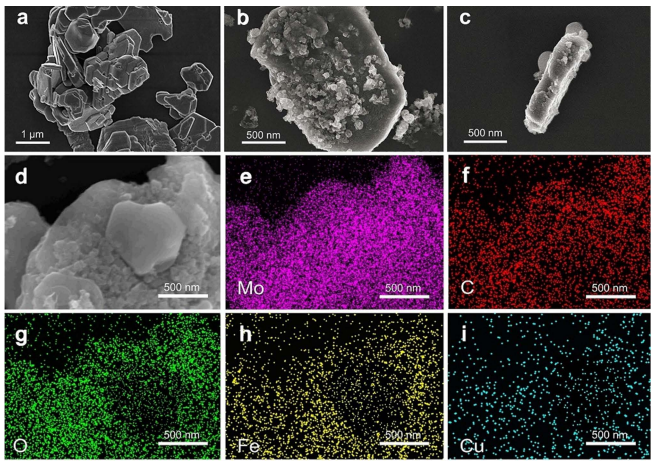

Figure 2 The SEM images of (a) Mo_2CT_x MXene and (b, c) $Cu/Fe_3O_4(1:3)/Mo_2CT_x$; (d—i) EDS mapping images of $Cu/Fe_3O_4(1:3)/Mo_2CT_x$.

spilled hydrogen atoms will migrate and readily react with WO_3, resulting in the formation of a blue compound, H_xWO_3. This reaction is characterized by the generation of d-d transitions of W^{5+} ions which appeared as an increase in absorbance in the ultraviolet-visible (UV-Vis) spectra at wavelengths of > 500 nm. The experimental results showed that after a 10-minute treatment with a 72% H_2/Ar mixture at 300 °C, samples containing copper species exhibited an enhanced absorbance, indicating the occurrence of H-spillover (Figure 3c), while the mixture of Fe_3O_4/Mo_2CT_x and WO_3 without Cu incorporation maintained its original color (Figure 3b). The catalysts with a higher copper content exhibited an increasingly intense blue color, which is indicative of a more pronounced spillover (Figures 3d and e).

The CO hydrogenation experiments were carried out for the Cu/Mo_2CT_x, $Cu/Fe_3O_4(1:1)/Mo_2CT_x$, $Cu/Fe_3O_4(1:3)/Mo_2CT_x$ and Fe_3O_4/Mo_2CT_x catalysts under both light irradiation and dark conditions using the same reactant gas ($CO/H_2/Ar$ = 24/72/4) at a catalyst bed temperature of 320 °C in a Harrick MRA-5 flow reactor. The effluent gas flow was analyzed online by an Agilent 990 micro-gas chromatograph (μGC) equipped with micro-thermal conductivity detectors (μTCD) to detect the CO hydrogenation products. Figures 4a and b present the CO conversion and the distributions of hydrocarbons for different catalysts. Compared to the dark condition, light irradiation dramatically enhanced the catalytic CO conversion using $Cu/Fe_3O_4/Mo_2CT_x$ and Fe_3O_4/Mo_2CT_x catalysts.[27] In the $Cu/Fe_3O_4/Mo_2CT_x$ catalysts, $Cu/Fe_3O_4(1:3)/Mo_2CT_x$ exhibited the highest catalytic activity for CO hydrogenation to C_{2+} hydrocarbons, reaching a CO conversion of 78.5% under light irradiation. Importantly, the addition of 5 wt% Cu into the Fe_3O_4/Mo_2CT_x catalysts led to an increase in both CO conversion and the yield of C_{2+} products under light irradiation and dark conditions. Notably, for the $Cu/Fe_3O_4(1:3)/Mo_2CT_x$ catalyst, the yield of C_2—C_3 hydrocarbons increased from 7.8% to 23.6% when light was introduced. As a catalyst support, Mo_2CT_x MXene revealed a low catalytic performance neither with nor without light irradiation (Figure S5).

Figure 4c illustrates the photothermal yields of C_2—C_3 hydrocarbons, CO conversion, and C_{2+} selectivity as a function of catalyst bed temperature using the $Cu/Fe_3O_4(1:3)/Mo_2CT_x$ catalyst. With an increase in temperature from 260 °C to 320 °C, both the yield of C_2—C_3 hydrocarbons and CO conversion increased. The C_{2+} selectivity among all hydrocarbons was nearly 70% at 260 °C. In Figure 4d, it can be observed that with increasing reaction pressure, the conversion of CO rises. This increase in pressure suppresses the selectivity towards CO_2 while enhancing the formation of C_{2+} hydrocarbons. This phenomenon arises due to the

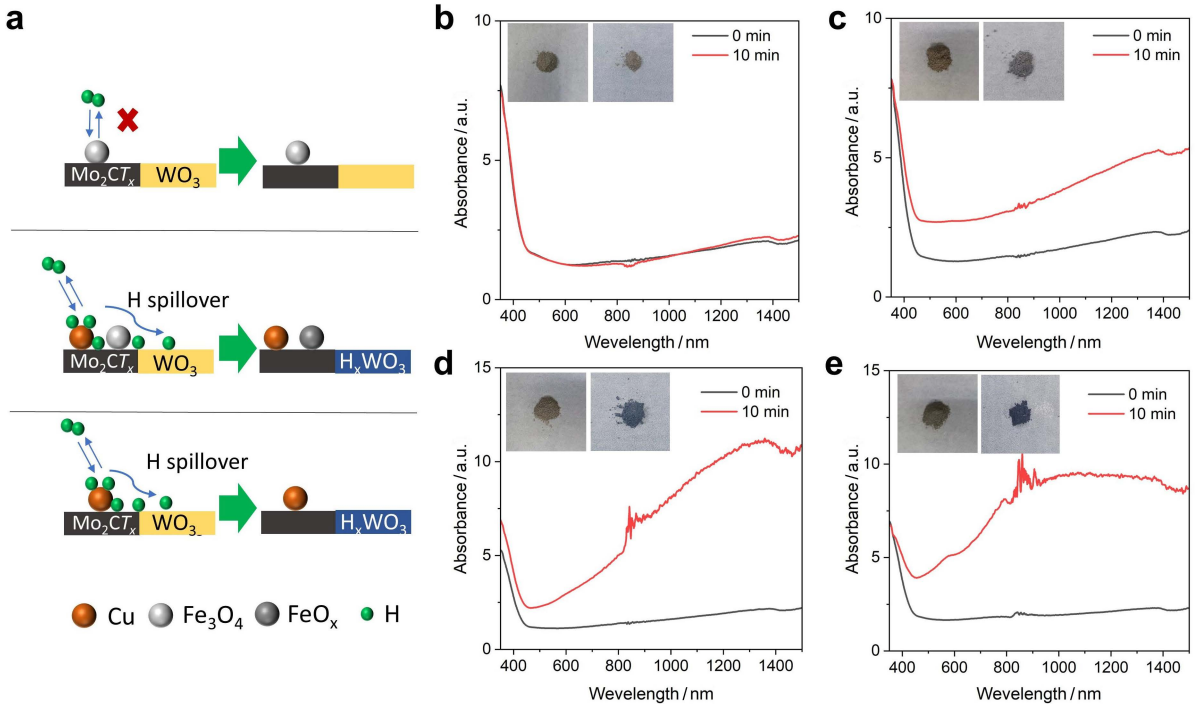

Figure 3 (a) Illustrative color change of the mixture of different catalysts with WO_3; UV-Vis spectra and photographs of the catalysts (b) Fe_3O_4/Mo_2CT_x, (c) $Cu/Fe_3O_4(1:3)/Mo_2CT_x$, (d) $Cu/Fe_3O_4(1:1)/Mo_2CT_x$, (e) Cu/Mo_2CT_x mixed with WO_3 before treatment (0 min) and after treatment with 72% H_2/Ar at 300 °C for 10 min.

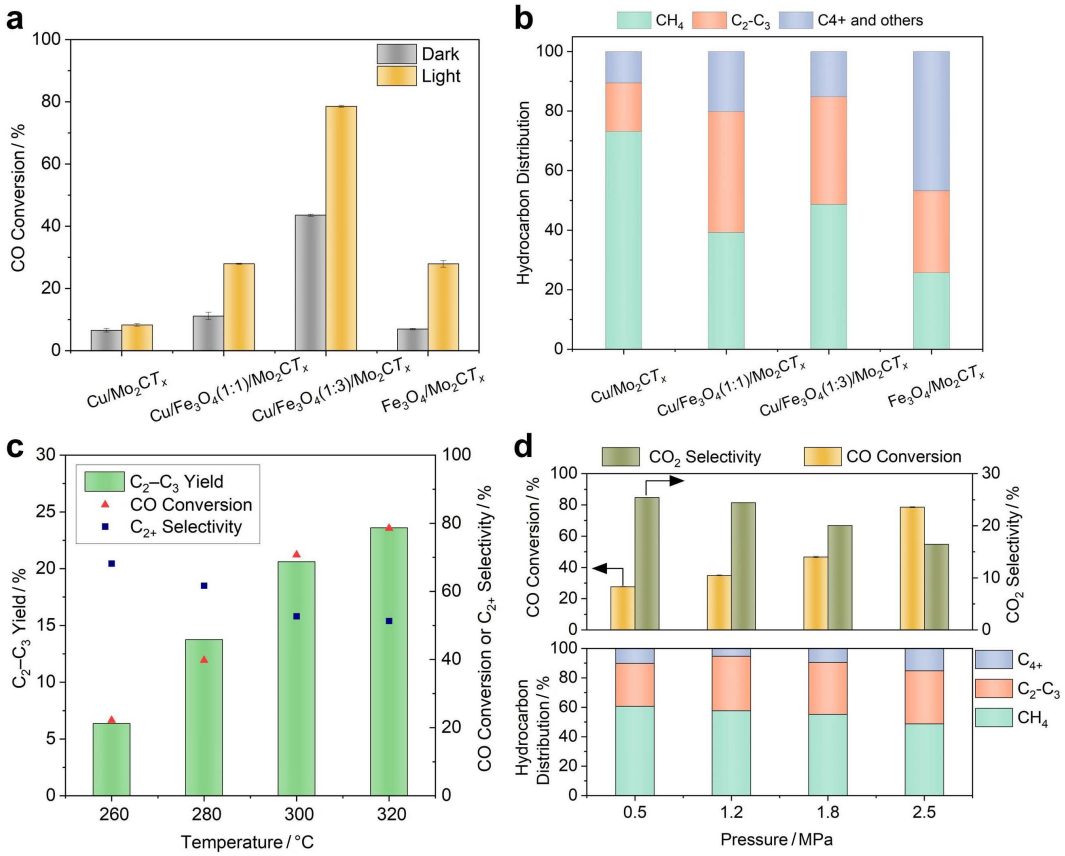

Figure 4 (a) CO conversion of different catalysts at 320 °C and 2.5 MPa with and without light irradiation; (b) hydrocarbons distribution of different catalysts with/without light irradiation at 320 °C and 2.5 Mpa; (c) C_2—C_3 yield, CO conversion, and C_{2+} selectivity of different catalysts as a function of reaction temperature at 2.5 MPa with light irradiation; (d) catalytic performance as a function of reaction pressure at 320 °C. Reaction conditions: $CO/H_2/Ar$ = 24/72/4, GHSV = 12000 $mL \cdot g_{cat}^{-1} \cdot h^{-1}$, 50 mg catalyst. Error bars represent standard deviations from three measurements.

reduction in the number of molecules involved in the CO-to-C_{2+} conversion. According to Le Chatelier's principle, C—C coupling becomes thermodynamically more favourable under pressurized conditions.[28] Two pathways for CO_2 formation had been investigated:[29-31] The first is the surface O* species formed by CO* dissociation reacting with another CO* to form CO_2, which also re-

acts with adsorbed hydrogen to form H_2O; and the second pathway is the water-gas shift (WGS) reaction of CO reactant with the primary H_2O product. As a result, at a relatively high pressure of 2.5 MPa, the C_{2+} yield reached 23.6% with a high C_{2+} selectivity of 51.3%, and the selectivity to CO_2 decreased to ~16%.

Light irradiation can increase the selectivity to CH_4, C_2H_6, and C_3H_8. One possible mechanism is that light irradiation accelerated the dissociation of H_2 into H* species with the co-existence of Cu^0 and Fe^0, which, in turn, promoted both the hydrogenation of $*CH_x$ species into CH_4 and C_2—C_3 hydrocarbons.[5,32-34]

As reported in previous studies,[8,35-38] the active Fe_5C_2 phases can be generated from Fe_3O_4 *in situ* during the reaction, originating from the reduction of Fe_3O_4 to metallic iron and subsequent carburization to Fe_5C_2, which serve as the pivotal sites for C_{2+} production in either thermal or photothermal reactions. Furthermore, Magnus Rønning *et al*.[17] observed that the formation of iron carbides can be facilitated by copper in the syngas atmosphere. Puga[38] emphasized the pronounced role of copper as a reduction promoter in iron catalysts. The H_2-TPR (Figure S6) results confirmed these opinions. The Fe_3O_4/Mo_2CT_x catalyst without Cu showed a peak at 362 °C, which can be ascribed to the transformation of Fe^{3+} to Fe^{2+}. The profile for the catalyst containing 5 wt% of Cu and 10 wt% of Cu showed that the peaks were shifted to lower temperatures at 275 °C, indicating that Cu loading promotes iron reduction. Metallic Cu crystallites start to nucleate early, providing dissociation sites for H_2 and hence increasing the concentration of atomic hydrogen on the catalyst surface to assist in the reduction of Fe species through H-spillover (Figure 3a). Therefore, it is reasonable to form low-crystallinity Fe_5C_2 during the reaction. The Fe $2p_{3/2}$ peak at 707.1 eV observed in the XPS spectra of the post-reaction $Cu/Fe_3O_4/Mo_2CT_x$ (Figure 1b), attributed to Fe^0 species, likely originates from the iron carbides species, thus having better CO hydrogenation ability.[39]

To investigate the stability, we conducted a long-time reaction over 35 h under light irradiation at 320 °C and 1.5 MPa using both $Cu/Fe_3O_4(1:3)/Mo_2CT_x$ and Fe_3O_4/Mo_2CT_x catalysts, confirming that the presence of Cu improved both the activity and stability (Figure S7). We also performed a series of cyclic experiments using the $Cu/Fe_3O_4(1:3)/Mo_2CT_x$ catalyst under 1-hour light irradiation at 350 °C and 0.3 MPa in a batch reactor without external heating, confirming that both the CO conversion and product selectivity remained consistent over 10 cycles (Figure S8). Post-reaction SEM results indicated that there were no significant changes in the surface morphology of the catalyst during the reaction (Figure S9). Additional characterizations, performance comparisons, and discussions are presented in Figures S10—S16 in the Supporting Information.

Conclusions

In summary, we have developed a robust $Cu/Fe_3O_4/Mo_2CT_x$ catalyst, significantly enhancing the C_{2+} production via photothermal CO hydrogenation. The Mo_2CT_x support efficiently converts incident light into heat to drive the photothermal reaction. The introduction of Cu, enhancing H_2 dissociation and H spillover, facilitates the *in situ* generation of active Fe^0 species in Fe_5C_2 during CO hydrogenation, increasing C_{2+} production. The $Cu/Fe_3O_4(1:3)/Mo_2CT_x$ catalyst achieved a high CO conversion of 78.5%, a C_2—C_3 hydrocarbon yield of 23.6%, and a C_{2+} selectivity of 51.3% under ~5.0 W cm^{-2} light irradiation at a catalyst bed temperature of 320 °C and a high gas hourly space velocity (GHSV) of 12000 $mL{\cdot}g_{cat}^{-1}{\cdot}h^{-1}$. The findings demonstrate that adding H_2 dissociation and H spillover promoter such as Cu can *in situ* promote the generation of Fe^0 in Fe_5C_2 active species, enabling efficient CO hydrogenation to C_{2+} products. Further research endeavors could explore the modification of the chemical states of active species during reactions to enhance C_{2+} production in photothermal FTS reactions.

Experimental

Catalyst synthesis: Multilayer Mo_2CT_x MXene was purchased from Xinxitechnology, Ltd. and used for the preparation of $Fe\text{-}Cu/Mo_2CT_x$. In a typical method, 100 mg Mo_2CT_x was first dispersed in 25 mL deionized water, followed by ultrasonication for 60 min. Then ferric chloride ($FeCl_3$) and copper chloride ($CuCl_2$) were added into the above suspension and stirred for 2 h at ambient temperature. Subsequently, excess $NaBH_4$ solution was rapidly added to the mixture to reduce Cu^{2+} and Fe^{3+} ions, and the resulting suspension was aged under stirring for 2 h. The product was collected by centrifugation, washed with deionized water for 3 times, and subsequently vacuum-dried overnight. Employing this synthesis method, four catalysts were prepared with varying Fe and Cu concentrations: 20 wt% Fe (Cat. Fe_3O_4/Mo_2CT_x), 15 wt% Fe combined with 5 wt% Cu (Cat. $Cu/Fe_3O_4(3:1)/Mo_2CT_x$), 10 wt% Fe combined with 10 wt% Cu (Cat. $Cu/Fe_3O_4(1:1)/Mo_2CT_x$), and 20 wt% Cu (Cat. Cu/Mo_2CT_x).

Characterization: The crystal structure and phase composition of the samples were determined by an X-ray powder diffractometer (XRD, Bruker Advantage D8 diffractometer with Cu Kα radiation and a D/teX Ultra detector). The surface morphology and microstructure of the samples were observed by scanning electron microscopy (SEM, Hitachi Regulus SU8100 instrument with an EDS analyzer) and Transmission Electron Microscope (TEM, FEI TALOS F200X at an accelerating voltage of 200 kV). The surface properties were determined by X-ray photoelectron spectroscopy (XPS) technique using a Thermo Scientific ESCA Lab250 spectrometer with an Al Kα monochromatic X-ray radiation source. The C 1s core level at 284.6 eV was taken as an internal reference to correct the shift of the binding energies. The ultraviolet-visible-near-infrared diffuse reflectance spectroscopy (UV-Vis-NIR DRS) was measured using a Shimazu UV3600Plus spectrometer in the wavelength range of 350—2500 nm with a $BaSO_4$ reference.

Photothermal CO hydrogenation: Photothermal CO hydrogenation experiments were performed using a Harrick (HVC-MRA5) flow reactor system (Figure S17). The prepared catalysts (50 mg) were placed into the reactor and pre-activated in 72% H_2 for 1 h at 350 °C and ambient pressure or in 5% H_2 for 2 h at 300 °C in a tube furnace. Subsequently, a reactant gas ($CO/H_2/Ar$ = 24/72/4, GHSV = 12000 $mL{\cdot}g_{cat}^{-1}{\cdot}h^{-1}$) was fed into the reactor and pressurized to 2.5 MPa. The catalytic reaction was carried out from 280 to 300 °C. A 300 W Xe lamp (CME-303, Microenerg Beijing Technology, equipped with a quartz guidance fiber) was used as the light source placed 9 mm above the reactor to implement light irradiation, and the light intensity is ~1.6 W. The surface temperature was measured by an infrared irradiation meter (SA-D5050A, Wuxi Shiao) under light irradiation. Agilent 990 micro-gas chromatograph (μGC) equipped with micro-thermal conductivity detectors (μTCD) was used to detect the CO hydrogenation products. The CO conversion, product selectivity, yield, and hydrocarbon distribution were calculated on a carbon atom basis according to the following Eqs. 1 to 4, respectively, where *F* is the molar flow rate of CO and product C_i (CO_2 and hydrocarbon; *i* represents carbon number).

$$\text{CO conversion} = \frac{F_{\text{CO, in}} - F_{\text{CO, out}}}{F_{\text{CO,in}}} \times 100\% \quad (1)$$

$$\text{Selectivity} = \frac{F_{\text{C}_i} \times i}{F_{\text{CO, in}} - F_{\text{CO, out}}} \times 100\% \quad (2)$$

$$\text{Yield} = \text{Selectivity} \times \text{CO conversion} \times 100\% \quad (3)$$

$$\text{Hydrocarbon distribution} = \frac{\text{Sel.}_{\text{C}_i\text{H}_j}}{\sum \text{Sel.}_{\text{C}_i\text{H}_j}} \quad (4)$$

Supporting Information

The supporting information for this article is available on the WWW under https://doi.org/10.1002/cjoc.202400905.

Acknowledgement

This work was supported by the National Natural Science Foundation of China (Grant Nos. 22272078, 2240090130), the National Key Research and Development Program of the Ministry of Science and Technology of China (No. 2020YFA0406102), the Frontiers Science Center for Critical Earth Material Cycling of Nanjing University, and the "Innovation and Entrepreneurship of Talents plan" of Jiangsu Province.

References

[1] Chen, G.; Syzgantseva, O. A.; Syzgantseva, M. A.; Yang, S.; Yan, G.; Peng, L.; Cao, C.; Chen, W.; Wang, Z.; Qin, F.; et al. Construction of Synergistic Co and Cu Diatomic Sites for Enhanced Higher Alcohol Synthesis. *CCS Chem*. **2023**, *5*, 851–864.

[2] Jiang, H.; Zhu, F.; Zhou, R.; Wang, L.; Xiao, Y.; Zhong, M. Promoted Photothermal Catalytic CO Hydrogenation by Using TiC-Supported Co−Fe_5C_2 Catalysts. *Chem. Eur. J.* **2023**, *29*, e202202891.

[3] Wang, Y.; Zhao, Y.; Liu, J.; Li, Z.; Waterhouse, G. I. N.; Shi, R.; Wen, X.; Zhang, T. Manganese Oxide Modified Nickel Catalysts for Photothermal CO Hydrogenation to Light Olefins. *Adv. Energy Mater.* **2020**, *10*, 1902860.

[4] Guo, X.-N.; Jiao, Z.-F.; Jin, G.-Q.; Guo, X.-Y. Photocatalytic Fischer–Tropsch Synthesis on Graphene-Supported Worm-Like Ruthenium Nanostructures. *ACS Catal.* **2015**, *5*, 3836–3840.

[5] Li, Z.; Liu, J.; Zhao, Y.; Waterhouse, G. I. N.; Chen, G.; Shi, R.; Zhang, X.; Liu, X.; Wei, Y.; Wen, X.-D.; et al. Co-Based Catalysts Derived from Layered-Double-Hydroxide Nanosheets for the Photothermal Production of Light Olefins. *Adv. Mater.* **2018**, *30*, 1800527.

[6] Jiang, H.; Wang, L.; Kaneko, H.; Gu, R.; Su, G.; Li, L.; Zhang, J.; Song, H.; Zhu, F.; Yamaguchi, A.; et al. Light-driven CO_2 methanation over Au-grafted $Ce_{0.95}Ru_{0.05}O_2$ solid-solution catalysts with activities approaching the thermodynamic limit. *Nat. Catal.* **2023**, *6*, 519–530.

[7] Gao, W.; Gao, R.; Zhao, Y.; Peng, M.; Song, C.; Li, M.; Li, S.; Liu, J.; Li, W.; Deng, Y.; et al. Photo-Driven Syngas Conversion to Lower Olefins over Oxygen-Decorated Fe_5C_2 Catalyst. *Chem* **2018**, *4*, 2917–2928.

[8] Li, Y.; Gao, W.; Peng, M.; Zhang, J.; Sun, J.; Xu, Y.; Hong, S.; Liu, X.; Liu, X.; Wei, M.; et al. Interfacial Fe_5C_2-Cu catalysts toward low-pressure syngas conversion to long-chain alcohols. *Nat. Commun.* **2020**, *11*, 61.

[9] Zhai, P.; Xu, C.; Gao, R.; Liu, X.; Li, M.; Li, W.; Fu, X.; Jia, C.; Xie, J.; Zhao, M.; et al. Highly Tunable Selectivity for Syngas-Derived Alkenes over Zinc and Sodium-Modulated Fe_5C_2 Catalyst. *Angew. Chem. Int. Ed.* **2016**, *55*, 9902–9907.

[10] Yu, X.; Xu, Y.; Li, L.; Zhang, M.; Qin, W.; Che, F.; Zhong, M. Coverage enhancement accelerates acidic CO_2 electrolysis at ampere-level current with high energy and carbon efficiencies. *Nat. Commun.* **2024**, *15*, 1711.

[11] Shi, Y.; Li, Z.; Hao, Q.; Li, R.; Li, Y.; Guo, L.; Ouyang, S.; Yuan, H.; Zhang, T. Hydrophobic Fe-Based Catalyst Derived from Prussian Blue for Enhanced Photothermal Conversion of Syngas to Light Olefins. *Adv. Funct. Mater.* **2024**, *34*, 2308670.

[12] Song, R.; Li, Z.; Guo, J.; Duchesne, P. N.; Qiu, C.; Mao. Guo, C.; Jing, D.; Ozin, G. A. Solar Hydrocarbons: Single-Step, Atmospheric-Pressure Synthesis of C_2–C_4 Alkanes and Alkenes from CO_2. *Angew. Chem. Int. Ed.* **2023**, *62*, e202304470.

[13] Xie, B.; Wong, R. J.; Tan, T. H.; Higham, M.; Gibson, E. K.; Decarolis, D.; Callison, J.; Aguey-Zinsou, K.-F.; Bowker, M.; Catlow, C. R. A.; et al. Synergistic ultraviolet and visible light photo-activation enables intensified low-temperature methanol synthesis over copper/zinc oxide/alumina. *Nat. Commun.* **2020**, *11*, 1615.

[14] Yang, H.; Dang, Y.; Cui, X.; Bu, X.; Li, J.; Li, S.; Sun, Y.; Gao, P. Selective synthesis of olefins via CO2 hydrogenation over transition-metal-doped iron-based catalysts. *Appl. Catal. B*: *Environ.* **2023**, *321*, 122050.

[15] Fang, C.; Wei, J.; Wang, R.; Ge, Q.; Xu, H. Catalytic Conversion of Syngas to Light Olefins over Cu-Fe based Catalyst. *J. Mol. Catal.* **2015**, *29*, 27–34.

[16] Liu, J.; Zhang, A.; Jiang, X.; Liu, M.; Sun, Y.; Song, C.; Guo, X. Selective CO_2 Hydrogenation to Hydrocarbons on Cu-Promoted Fe-Based Catalysts: Dependence on Cu–Fe Interaction. *ACS Sustainable Chem. Eng.* **2018**, *6*, 10182–10190.

[17] Peña, D.; Jensen, L.; Cognigni, A.; Myrstad, R.; Neumayer, T.; van Beek, W.; Rønning, M. The Effect of Copper Loading on Iron Carbide Formation and Surface Species in Iron-Based Fischer–Tropsch Synthesis Catalysts. *ChemCatChem* **2018**, *10*, 1300–1312.

[18] Li, W.; Jiang, H.; Zhang, X.; Lei, B.; Li, L.; Zhou, H.; Zhong, M. Sustainable Electrosynthesis of *N*,*N*-Dimethylformamide via Relay Catalysis on Synergistic Active Sites. *J. Am. Chem. Soc.* **2024**, *146*, 21968–21976.

[19] Zhao, J.; Bai, Y.; Liang, X.; Wang, T.; Wang, C. Photothermal catalytic CO_2 hydrogenation over molybdenum carbides: Crystal structure and photothermocatalytic synergistic effects. *J. CO_2 Util.* **2021**, *49*, 101562.

[20] Deeva, E. B.; Kurlov, A.; Abdala, P. M.; Lebedev, D.; Kim, S. M.; Gordon, C. P.; Tsoukalou, A.; Fedorov, A.; Müller, C. R. *In Situ* XANES/XRD Study of the Structural Stability of Two-Dimensional Molybdenum Carbide Mo_2CT_x: Implications for the Catalytic Activity in the Water–Gas Shift Reaction. *Chem. Mater.* **2019**, *31*, 4505–4513.

[21] Peng, W.; Luo, M.; Xu, X.; Jiang, K.; Peng, M.; Chen, D.; Chan, T.-S.; Tan, Y. Spontaneous Atomic Ruthenium Doping in Mo_2CT_X MXene Defects Enhances Electrocatalytic Activity for the Nitrogen Reduction Reaction. *Adv. Energy Mater.* **2020**, *10*, 2001364.

[22] Zhou, H.; Chen, Z.; Kountoupi, E.; Tsoukalou, A.; Abdala, P. M.; Florian, P.; Fedorov, A.; Müller, C. R. Two-dimensional molybdenum carbide 2D-Mo_2C as a superior catalyst for CO_2 hydrogenation. *Nat. Commun.* **2021**, *12*, 5510.

[23] Morales-García, Á.; Fernández-Fernández, A.; Viñes, F.; Illas, F. CO abatement using two-dimensional MXene carbides. *J. Mater. Chem. A* **2018**, *6*, 3381–3385.

[24] Zhou, H.; Chen, Z.; López, A. V.; López, E. D.; Lam, E.; Tsoukalou, A.; Willinger, E.; Kuznetsov, D. A.; Mance, D.; Kierzkowska, A.; et al. Engineering the Cu/Mo_2CT_x (MXene) interface to drive CO_2 hydrogenation to methanol. *Nat. Catal.* **2021**, *4*, 860–871.

[25] Yamashita, T.; Hayes, P. Analysis of XPS spectra of Fe^{2+} and Fe^{3+} ions in oxide materials. *Appl. Surf. Sci.* **2008**, *254*, 2441–2449.

[26] Yue, Y.; Liu, B.; Qin, P.; Lv, N.; Wang, T.; Bi, X.; Zhu, H.; Yuan, P.; Bai, Z.; Cui, Q.; et al. One-pot synthesis of FeCu-SSZ-13 zeolite with superior performance in selective catalytic reduction of NO by NH_3 from natural aluminosilicates. *Chem. Eng. J.* **2020**, *398*, 125515.

[27] Xu, D.; Li, Z.; Li, L.; Wang, J. Insights into the Photothermal Conversion of 2D MXene Nanomaterials: Synthesis, Mechanism, and Applications. *Adv. Funct. Mater.* **2020**, *30*, 2000712.

[28] Pastor-Pérez, L.; Baibars, F.; Le Sache, E.; Arellano-García, H.; Gu, S.; Reina, T. R. CO_2 valorisation via Reverse Water-Gas Shift reaction using advanced Cs doped Fe-Cu/Al_2O_3 catalysts. *J. CO_2 Util.* **2017**, *21*, 423–428.

[29] Krishnamoorthy, S.; Li, A.; Iglesia, E. Pathways for CO_2 Formation and Conversion During Fischer–Tropsch Synthesis on Iron-Based Catalysts. *Catal. Lett.* **2002**, *80*, 77–86.

[30] Liu, B.; Li, W.; Zheng, J.; Lin, Q.; Zhang, X.; Zhang, J.; Jiang, F.; Xu, Y.; Liu, X. CO_2 formation mechanism in Fischer–Tropsch synthesis over iron-based catalysts: a combined experimental and theoretical study. *Catal. Sci. Technol.* **2018**, *8*, 5288–5301.

[31] Wang, P.; Chen, W.; Chiang, F.-K.; Dugulan, A. I.; Song, Y.; Pestman, R.; Zhang, K.; Yao, J.; Feng, B.; Miao, P.; et al. Synthesis of stable and low-CO_2 selective iron-carbide Fischer-Tropsch catalysts. *Sci. Adv.* **2018**, *4*, eaau2947.

[32] Liu, L.; Puga, A. V.; Cored, J.; Concepción, P.; Pérez-Dieste, V.; García, H.; Corma, A. Sunlight-assisted hydrogenation of CO_2 into ethanol and C_{2+} hydrocarbons by sodium-promoted Co@C nanocomposites. *Appl. Catal. B: Environ.* **2018**, *235*, 186–196.

[33] Zhang, H.; Dong, A.; Liu, B.; Chen, J.; Xu, Y.; Liu, X. Hydrogen spillover effects in the Fischer–Tropsch reaction over carbon nanotube supported cobalt catalysts. *Catal. Sci. Technol.* **2023**, *13*, 1888–1904.

[34] Li, L.; Liu, Z.; Yu, X.; Zhong, M. Achieving High Single-Pass Carbon Conversion Efficiencies in Durable CO_2 Electroreduction in Strong Acids via Electrode Structure Engineering. *Angew. Chem. Int. Ed.* **2023**, *62*, e202300226.
[35] Li, Z.; Wu, W.; Wang, M.; Wang, Y.; Ma, X.; Luo, L.; Chen, Y.; Fan, K.; Pan, Y.; Li, H.; et al. Ambient-pressure hydrogenation of CO_2 into long-chain olefins. *Nat. Commun.* **2022**, *13*, 2396.
[36] Xiao, K.; Bao, Z.; Qi, X.; Wang, X.; Zhong, L.; Fang, K.; Lin, M.; Sun, Y. Structural evolution of CuFe bimetallic nanoparticles for higher alcohol synthesis. *J. Mol. Catal. A Chem.* **2013**, *378,* 319–325.
[37] Li, S.; Meitzner, G. D.; Iglesia, E. Structure and Site Evolution of Iron Oxide Catalyst Precursors during the Fischer–Tropsch Synthesis. *J. Phys. Chem. B* **2001**, *105*, 5743–5750.
[38] Puga, A. V. On the nature of active phases and sites in CO and CO_2 hydrogenation catalysts. *Catal. Sci. Technol.* **2018**, *8*, 5681–5707.
[39] Li, R.; Li, Y.; Li, Z.; Wei, W.; Hao, Q.; Shi, Y.; Ouyang, S.; Yuan, H.; Zhang, T. Electronically Activated Fe_5C_2 via N-Doped Carbon to Enhance Photothermal Syngas Conversion to Light Olefins. *ACS Catal.* **2022**, *12*, 5316–5326.

Manuscript received: August 25, 2024
Manuscript revised: December 9, 2024
Manuscript accepted: December 26, 2024
Version of record online: January 28, 2025

The Authors

Left to Right: Renjie Zhou, Haoyang Jiang, Yongcheng Xiao, Yueren Liu and Miao Zhong

